PLANNING THE VELOCITY OF A PARALLEL HYBRID ELECTRIC IN VEHICLE-TO-VEHICLE AUTONOMOUS DRIVING: AN OPTIMIZATION-BASED APPROACH

Pier Giuseppe Anselma [1,2]

[1]*Department of Mechanical and Aerospace Engineering (DIMEAS)*
Politecnico di Torino, Torino, Italy (E-mail: pier.anselma@polito.it)
[2]*Center for Automotive Research and Sustainable Mobility (CARS)*
Politecnico di Torino, Torino, Italy

ABSTRACT: Improved numerical tools are required to foster flexible and effective advancement of innovative electrified and highly automated road vehicles. This paper proposes an optimization-based approach to off-line plan the longitudinal velocity of a hybrid electric vehicle (HEV) when travelling as Ego vehicle in a vehicle-to-vehicle (V2V) autonomous driving scenario. A parallel P2 hybrid powertrain layout is retained along with the corresponding on-board supervisory controller. A mathematical formulation for the optimal V2V autonomous driving control problem is provided and consequently solved with an optimization method based on dynamic programming (DP). The implemented DP formulation particularly exploits information about the overall longitudinal speed profile of a Lead vehicle in a predefined driving mission to determine the velocity profile of the Ego vehicle. Optimization constraints involve maintaining the inter-vehicular distance value within allowed limits while aiming at minimizing both the magnitude of Ego vehicle acceleration events and the overall Ego vehicle fuel consumption as predicted according to the on-board hybrid supervisory control logic. Simulation results for different driving missions demonstrate that, using the proposed DP formulation, the Ego vehicle can achieve both smoother speed profiles and improved fuel economy by some percentage points in V2V autonomous driving compared to the retained Lead vehicle embedding the same HEV powertrain layout.

KEY WORDS: autonomous driving, electrified powertrain, hybrid electric vehicle (HEV), optimal control, vehicle-to-vehicle, velocity planning

1. Introduction

Automation and electrification currently represent well-established development trends in the automotive field. Improved numerical tools are required to foster flexible and effective advancement of these innovative electrified and highly automated road vehicles [1]. However, research activities concerning vehicle automation are usually decoupled from their counterparts involving vehicle electrification due to both the increased level of complexity and the partitioned organization of automotive OEMs. In this framework, implementing vehicle development approaches involving simultaneously electrification and automation would result beneficial both in facilitating the overall vehicle design procedure and in exploiting most advantage from both the development topics. Focusing on fuel economy, a related example would concern planning the longitudinal speed trajectory for an automated vehicle while minimizing the overall fuel consumption according to the specific propulsion system layout embedded on-board [2].

Concerning vehicle automation, a short-term effective solution can be identified in developing automated driving strategies based on vehicle-to-vehicle (V2V) communication. When compared to other vehicular technologies such as vehicle-to-infrastructure communication (V2I), vehicle-to-grid communication (V2G) or vehicle-to-pedestrian communication (V2P), the relative ease of implementation of V2V communication represents a major drive in this framework [3][4]. As example, Toyota and Lexus recently announced the implementation of Dedicated Short-Range Communications (DSRC) systems for V2V interaction on vehicles sold in the United States starting in 2021 [5]. Figure 1 illustrates a sketch of a V2V autonomous driving scenario involving two vehicles, where the preceding and the following vehicles are named as 'Lead vehicle' and 'Ego vehicle' respectively. The Lead vehicle can be either human-operated or automated, while the Ego vehicle is controlled by automated driving. The Ego vehicle follows the Lead vehicle and the inter-vehicular distance (IVD) between them varies over time. The Ego vehicle receives information from the Lead vehicle regarding its position (x_{lead}), its longitudinal speed ($\dot{x}_{lead}$) and its longitudinal acceleration ($\ddot{x}_{lead}$) as example.

As regards powertrain electrification, current limits in economical availability of large on-board electrical energy storage and in rapid charging infrastructure restrain the widespread adoption of

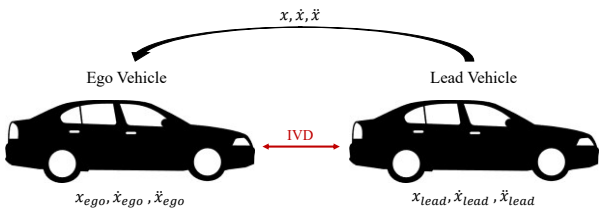

Figure 1. V2V autonomous driving scenario.

pure electric vehicles [6]. Contrarily, hybrid electric vehicles (HEVs) represent an ongoing promising technology to reduce fuel consumption and tailpipe emissions while avoiding wide dependence on electrical charging infrastructure [7]. In this framework, a compelling need can be identified in implementing research and development tools to foster HEVs that efficiently operate in V2V autonomous driving mode. Recent research efforts have demonstrated the capability of improving fuel economy by exploiting information coming from the Lead vehicle in a V2V communication scenario. As example, neural networks have been used in 2017 to predict the velocity of the ego vehicle and adjust the equivalence factor for the usage of battery energy in a HEV [8]. In 2018, an on-board real-time HEV controller based on off-line optimization of the Ego vehicle speed profile while detecting physical constraints through V2V and V2I communication was proposed for a P0-P4 parallel HEV powertrain [9]. A recent study claimed that up to 6 % improvement of fuel economy would be possible for a power-split HEV powertrain by predicting the upcoming 120 seconds of the ego vehicle speed profile by means of V2V communication [10].

Despite the presence of the studies reviewed above, in the author's opinion, the advancement of energy management strategies for HEV powertrains through the exploitation of information coming from V2V communication still needs exhaustive exploration and represents an open research question. This paper therefore aims at introducing an off-line optimal algorithm for planning the velocity profile of an ego HEV in a V2V autonomous driving scenario for the overall driving mission with the aim of improving on-board energy flows. The proposed algorithm is based on dynamic programming (DP), a popular approach based on the concept of global optimality, and exploits information coming from both the embedded on-board HEV control strategy and the Lead vehicle in V2V autonomous driving to evaluate the optimal longitudinal speed trajectory of the Ego vehicle. Other than improving on-board HEV energy management and fuel economy, the proposed approach is suggested improving passenger comfort for the Ego vehicle by reducing the magnitude of longitudinal acceleration and deceleration events. The rest of this paper is organized as follows: the retained HEV powertrain layout is firstly presented and modeled and its on-board supervisory controller is outlined. The subsequent section then describes the proposed workflow for optimally deriving the speed profile for the HEV as ego vehicle in an off-line V2V autonomous driving scenario. Simulation results are then presented, and conclusions are drawn.

2. Retained HEV

This section illustrates the retained HEV and its numerical model, then the corresponding hybrid supervisory controller is outlined.

2.1. Parallel P2 HEV

In this study, a parallel P2 HEV powertrain configuration has been retained. Among the different architectures, parallel HEVs have been selected by many car manufacturers as their first step into vehicle electrification. In a parallel HEV, the tractive power is combined: both the internal combustion engine (ICE) and the electric motor/generator (MG) can contribute to the vehicle propulsion, i.e. their corresponding torques are additive. When the MG is large enough, it can drive the HEV by itself or simultaneously with the ICE. The MG, by motoring or generating, can also be used to shift the ICE to higher-efficiency operating points. The parallel P2 HEV architecture retained in this paper is illustrated in Figure 2. One MG is placed between the ICE and the gearbox input, while a clutch connection allows the ICE crankshaft to be disengaged from the MG and the rest of the vehicle drivetrain. Among the parallel HEV powertrain configurations, P2 has indeed been demonstrated promising in terms of energetic efficiency over a wide range of different driving scenarios [11]. Parameters for the HEV under study have been reported in Table 1. In general, chassis and power components data (e.g. ICE, MG, battery) for a full hybrid electric compact vehicle have been generated using the corresponding numerical tools available in Amesim® software [12]-[15]. A 5-speed automated manual transmission (AMT) is embedded in the considered HEV. In general, the presented HEV numerical model and supervisory controller find implementation in MATLAB® software.

Table 1. HEV parameters

Component	Parameter	Value
Vehicle	m_{veh}	1360 kg
	r_{dyn}	0.298 m
	μ_{roll}	0.025
	μ_{misc}	1 N/(m/s)
	ρ_{air}	1.2 kg/m^3
	c_x	0.29
	A_{fr}	2.24 m^2
ICE	Capacity	2.0 l
	Type	4-cylinders in-line, spark-ignition, naturally aspired
	Maximum power	89 kW @ 5000 rpm
	Maximum torque	174 Nm @ 4500 rpm
	Peak efficiency	30.5 %
Transmission	Gear ratios	[3.45; 1.85; 1.36; 1.07; 0.8]
	Final drive ratio	4.83
MG	Maximum power	43 kW
	Maximum torque	208 Nm
Battery pack	Pack configuration	240S 1P
	Nominal capacity	6.5 Ah
	Nominal voltage	310 V

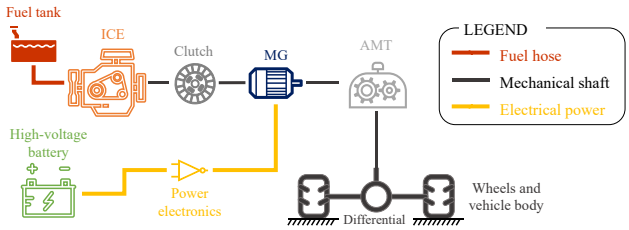

Figure 2. Parallel P2 HEV powertrain.

2.2. Numerical modeling

A backward quasi-static approach is retained here when modeling the HEV powertrain. The quasi-static approach considers constant time intervals and works back-ward deriving the value of needed propelling torque from vehicle speed values in adjacent time points [16]. Particularly, the value of required torque at the input shaft of the differential T_{IN} can be determined at each time instant of the driving mission as:

$$T_{IN} = \frac{(\mu_{roll} \cdot m_{veh} \cdot g + \mu_{misc} \cdot \dot{x} + 0.5 \cdot \rho_{air} \cdot c_x \cdot A_{fr} \cdot \dot{x}^2 + m_{veh} \cdot \ddot{x}) \cdot r_{dyn}}{i_{FD}} \quad (1)$$

where m_{veh}, $\dot{x}$, $\ddot{x}$, r_{dyn} and i_{FD} respectively represent the vehicle mass, the vehicle speed, the vehicle acceleration (as evaluated from values of vehicle speed in adjacent time instants), the wheel dynamic radius and the final drive ratio. μ_{roll} and g are the rolling resistance coefficient and the gravity acceleration, respectively. μ_{misc} represents the vehicle coefficient of viscous friction, and it considers miscellaneous terms (e.g. side forces, transmission losses) which linearly depend on the value of vehicle speed. ρ_{air} is the air density, while c_x and A_{fr} stand for the vehicle aerodynamic drag coefficient and frontal area, respectively.

After T_{IN} is known, determining the torque acting on each power component becomes possible by means of the torque balance relationship illustrated in equation (2) for the parallel P2 HEV:

$$T_{ICE} + T_{MG} = \frac{T_{IN}}{i_{gear}(j)} \quad (2)$$

where T_{ICE} and T_{MG} correspond to the torque values provided by the ICE and the MG, respectively. i_{gear} represents the gear ratio related to the gear number engaged at the generic time instant *j*.

As concerns the electrical energy path, the amount of power that the battery is requested to either deliver or absorb (P_{batt}) can be determined as:

$$P_{batt} = \frac{P_{MG}}{[\eta_{MG}(\omega_{MG}, T_{MG})]^{sign(P_{MG})}} \quad (3)$$

where P_{MG} and η_{MG} respectively represent the mechanical power and the overall efficiency of the MG, which is evaluated by means of an empirical lookup table with speed and torque as independent variables. Retaining the sign of P_{MG} as exponent in the denominator allows capturing both depleting and charging battery conditions within this formula. The rate of battery state-of-charge (SOC) can then be evaluated by considering an equivalent open circuit model as in equation (4):

$$\dot{SOC} = \frac{V_{OC}(SOC) - \sqrt{[V_{OC}(SOC)]^2 - 4 \cdot R_{IN}(SOC) \cdot P_{batt}}}{2 \cdot R_{IN}(SOC) \cdot Q_{batt}} \quad (4)$$

where V_{OC} and R_{IN} are the open-circuit voltage and the internal resistance of the battery pack, as obtained by interpolating in 1D lookup tables with SOC ad independent variable. Q_{batt} represents the battery pack capacity in ampere-seconds.

Concerning the ICE, the instantaneous rate of fuel consumption can be evaluated using an empirical steady-state lookup table with torque and speed as independent input variables.

2.3. Hybrid supervisory controller

Energy management systems, also known as hybrid supervisory controllers, represent a crucial aspect of HEVs. These controllers perform vehicle-level management tasks involving the repartition of requested power from the driver among components of the hybrid electric powertrain. Moreover, they aim at effectively supervise some fundamental vehicle states such as the battery SOC, the overall fuel consumption and the emission of pollutants. When controlling a parallel P2 HEV, three levels of decisions need to be made at each time instant by the hybrid supervisory controller [17]:

1. Which gear is to be engaged in the gearbox;
2. Whether to propel the HEV in pure electric mode (MG only) or in hybrid operation (both ICE and MG operating);
3. In case the hybrid mode is selected, how is the required torque split between the ICE and MG.

Currently, the most popular control method implemented as on-board hybrid supervisory controllers in HEVs relates to heuristic approaches [18]. In this work, a map-based heuristic method is retained as hybrid supervisory controller for the HEV under analysis. The considered hybrid supervisory controller is particularly inherited from Amesim® software, where a calibration procedure has already been performed for the parallel P2 HEV layout under study [19]. At each time instant, the gear to be engaged in the gearbox is decided upon the current value of vehicle speed. Then, current values for battery SOC, vehicle speed $\dot{x}$ and requested input power at the gearbox input shaft P_{IN} are considered for determining pure electric or hybrid electric operation. The workflow illustrated in Figure 3 finds implementation in this framework. In particular The ICE is set to be in operation at the given drive cycle time instant if at least one

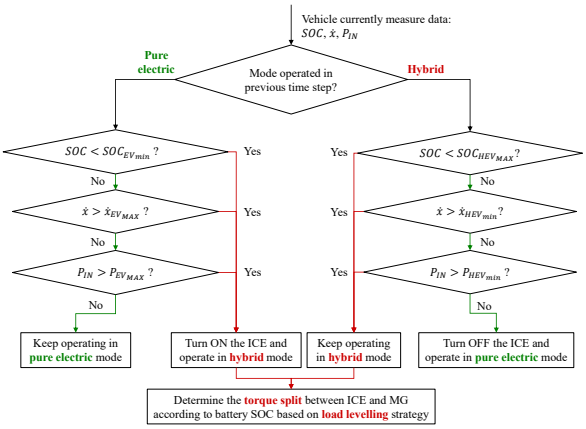

Figure 3. Algorithm for selecting pure electric or hybrid operation at each time instant.

Table 2. Hybrid supervisory control parameters

Variable	Operating mode in previous time instant	Parameter	Value
SOC	EV	$SOC_{EV_{min}}$	0.40
	HEV	$SOC_{HEV_{MAX}}$	0.80
Vehicle speed	EV	$\dot{x}_{EV_{MAX}}$	45 km/h
	HEV	$\dot{x}_{HEV_{min}}$	11 km/h
Requested power	EV	$P_{EV_{MAX}}$	40 kW
	HEV	$P_{HEV_{min}}$	0 kW

of the following criteria is met: (1) the battery SOC is below a certain threshold (SOC_{EV-min} or $SOC_{HEV-MAX}$), (2) the vehicle speed is greater than a given threshold ($\dot{x}_{EV-MAX}$ or $\dot{x}_{HEV-min}$), or (3) the requested power is higher than a predefined value (P_{EV-MAX} or $P_{HEV-min}$). Subscripts 'EV' or 'HEV' refer to the ICE being already activated or disactivated for the current time instant, respectively. Values of thresholds selected here for the hybrid supervisory controller parameters are reported in Table 2. As it can be noticed in Table 2, different threshold values are retained for SOC, vehicle speed and requested power depending on the operating mode at the previous drive cycle time instant. In particular, the following relationships hold to prevent too much frequent ICE de/activation events: $SOC_{EV-min} < SOC_{HEV-MAX}$, $\dot{x}_{EV-MAX} > \dot{x}_{HEV-min}$ and $P_{EV-MAX} > P_{HEV-min}$.

As a backup condition, the ICE is set to be activated and to provide the required supplementary torque in case the MG is not capable of delivering the requested propelling torque alone in pure electric mode. In case the hybrid mode is selected to operate for the current time instant, the last step in Figure 3 involves determining the torque split between ICE and MG of the considered P2 full HEV. Here, a commonly heuristic approach is considered in determining the torque split according to the current value of battery SOC. The considered HEV is a full hybrid which does not involve charging the battery from the external electricity grid. The high-voltage battery is therefore controlled to overall operate in charge-sustaining mode. Considering a reference SOC value of 60%, higher values of torque can be set to be delivered by the ICE as the battery SOC value for the corresponding time instant becomes progressively lower than 60% [20]. Battery charge-sustenance can be ensured in this way on the drive cycle time horizon.

3. Off-line optimal V2V autonomous driving

Once the retained P2 HEV modeling approach and hybrid supervisory controller have been presented in the previous section, this section aims at introducing and solving the optimal V2V autonomous driving problem.

3.1. Optimal V2V autonomous driving problem

In the V2V autonomous driving scenario illustrated in Figure 1, the Ego vehicle receives at each time instant information from the Lead vehicle including its position x_{lead}, velocity $\dot{x}_{lead}$, and acceleration $\ddot{x}_{lead}$, respectively. The communication between the two vehicles is supposed ideal, and a given value of inter-vehicular distance (IVD) results from the positions, speeds and accelerations of both Lead vehicle and Ego vehicle at each time instant. Two optimization targets are considered here for the Ego vehicle respectively related to the propelling energy minimization and the passenger comfort enhancement. The mathematical formulation corresponding to the optimal cooperative driving problem under analysis has been derived and it is reported in equation (5):

$$\min\left\{J_{ego}(\ddot{x}_{ego}) = \int_{t_0}^{t_{end}} \left[\alpha \cdot P_{traction-chem}(\ddot{x}_{ego}, t) + (1-\alpha)\cdot \ddot{x}_{ego}^2(t)\right] dt\right\} \quad (5)$$

With:

$$P_{traction-chem}(\ddot{x}_{ego}, t) = LHV_{fuel} \cdot \left[\dot{m}_{fuel}(\ddot{x}_{ego}, t) + m_{fuel-crank} \cdot start_{ICE}(\ddot{x}_{ego}, t)\right] - V_{OC}\cdot Q_{batt} \cdot \dot{SOC}(\ddot{x}_{ego}, t)$$

Subject to:

$$\left[x_{lead}(t) - x_{ego}(t)\right] \le IVD_{MAX}(t)$$

$$\left[x_{lead}(t) - x_{ego}(t)\right] \ge IVD_{safety}(t)$$

$$\ddot{x}_{ego}(t) \le \ddot{x}_{ego-MAX}\left[\dot{x}_{ego}(t)\right]$$

where J_{ego} represents the cost function for the Ego vehicle V2V automated driving that depends on the controlled Ego vehicle acceleration. The value of J_{ego} that needs minimization represents an integration of the instantaneous cost terms throughout the entire drive cycle form the initial time instant t_0 to the final time instant t_{end}. $P_{traction-chem}$ is the chemical power used for propelling the Ego vehicle and it relates to both fuel and electricity. This term varies over time and it depends on the controlled Ego vehicle acceleration. $P_{traction-chem}$ can be evaluated by considering the hybrid supervisory controller previously detailed and embedding it within the optimization problem. Thanks to this approach, improving the Ego HEV on-board energy management can be achieved when generating the corresponding longitudinal speed profile over time. LHV_{fuel} is the lower heating value of the fuel and corresponds to 42700 joules/grams. $\dot{m}_{fuel}$ represents the ICE fuel rate in grams/second obtained by interpolating in the steady-state fuel consumption lookup table as function of ICE speed and torque, while $m_{fuel-crank}$ is the mass of fuel required to crank the engine in grams. $start_{ICE}$ is a binary flag detecting ICE activations, and its value is set to 1 in those time instants in which the fuel consumption exhibits positive values while it was 0 in previous time instants. The term $V_{OC}\cdot Q_{batt}\cdot \dot{SOC}$ stands for the battery electrical power, while α represents a coefficient for weighting the optimal control targets as discussed below. The reported cost function formulation allows expressing both the fuel chemical power term and the battery electrical power term in watts. Other than propelling energy reduction, enhancement of the comfort of the ride represents a crucial potential of autonomous driving. To foster this aspect, several motion, path, and velocity planners proposed in literature integrate as objective minimization of values of variables related to vehicle longitudinal acceleration, lateral acceleration and yaw rate as for example in [21]-[23]. Following a similar approach, reduction of the root mean square (RMS) of the Ego vehicle acceleration $\ddot{x}_{ego}$ over the entire simulated drive cycle is considered here as evaluation metric to enhance the passenger comfort [24]. Reducing the overall energy used for propulsion and improving the passenger comfort might eventually represent contrasting objectives. As example, in electrified vehicles several fluctuations can be observed in the longitudinal speed when optimizing for energy consumption solely [25]. A trade-off between the two optimization targets retained might thus be implied in this framework by properly tuning the weighting coefficient α.

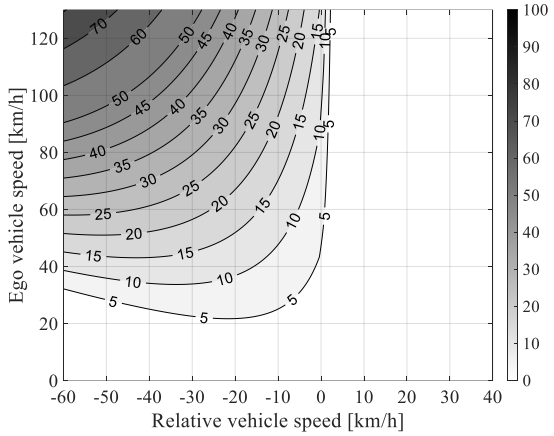

Figure 4. Minimum safety IVD as a function of the Ego vehicle speed and the relative vehicle speed between Lead vehicle and Ego vehicle.

Three additional requirements are involved in the constraints set for the optimization problem. First, the technological limitations in the V2V communication capability and the road utilization need consideration. Both these objectives are summarized here in imposing the IVD to always remain within the maximum allowed limit IVD_{MAX}. A variable value depending on the road type is considered in this work for IVD_{MAX}. As a general consideration, the IVD might be limited in urban areas to ease traffic flow and to reduce general road occupancy. This correlates well with reduced values of vehicle speed generally associated with urban driving. Contrarily, larger road surface availability and generally higher values of vehicle speed might lead to allow a higher value of IVD_{MAX} in extra-urban and highway driving conditions. In light of these considerations, when extra-urban and highway driving conditions are encountered, the maximum achievable value of IVD is set here to 300 meters which refers to the current approximate range of V2V communication [26]. On the other hand, the value of IVD_{MAX} is reduced to 40 meters in urban driving conditions in order to limit road occupancy [25].

As regards the minimum safety IVD, its value is obtained by interpolating in a two-dimensional lookup table with Following vehicle speed and relative vehicle speed between Preceding vehicle and Following vehicle as independent variables. The lookup table considered here is shown in Figure 4 and it is derived from a time-headway numerical braking model proposed in [27]. The interested reader can consult [25] for further information regarding this procedure.

Finally, the third optimization constraint involves limiting the Ego vehicle acceleration below the maximum limit given as a function of the maximum tractive power of the retained powertrain, which in turn depends on the maximum power capability of the embedded power components and on the current value of vehicle velocity.

3.2. Optimization-based Ego vehicle velocity planner

In this sub-section, a methodology to find the optimal control solution for the Ego vehicle V2V autonomous driving problem detailed above finds discussion. Dynamic programming (DP) is implemented in this context as a popular technique that can identify the optimal solution for multi-stage control and decision making problems [28][29]. To achieve this target, DP requires the knowledge of the Lead vehicle speed profile over time for the entire driving mission a priori before running the optimization process. The optimal control solution for the Ego vehicle V2V autonomous driving problem is then identified by DP by exhaustively sweeping all possible discretized control actions while solving an optimization problem backwardly form the final time instant t_{end} to the initial one t_0 of the considered drive cycle [30][31]. The optimal sequence of control actions is thus identified by minimizing the overall value of the predefined cost function.

DP requires the definition of the control variable set U and the state variable set X. U includes all the control variables associated to the considered control problem, while X includes the variables whose evolution over time need to be monitored throughout the considered control horizon (i.e. the entire driving mission). Control variable set and state variable set for the considered optimal Ego vehicle V2V autonomous driving problem are reported in equation (6).

$$U = \{\ddot{x}_{ego}(t)\},\ X = \begin{Bmatrix} IVD(t) \\ \dot{x}_{ego}(t) \\ ICE_{state}(t) \end{Bmatrix} \tag{6}$$

The Ego vehicle longitudinal acceleration needs to be controlled in this case, while the state space includes the IVD and the Ego vehicle speed $\dot{x}_{ego}$. The IVD is particularly considered to ensure the compliance over time with the corresponding optimization constraints, while the Ego vehicle longitudinal velocity is retained to evaluate its trajectory over time by integrating the controlled Ego vehicle longitudinal acceleration over time. Finally, the binary variable for the ICE state ICE_{state} is retained that corresponds to hybrid or pure electric operation. Monitoring ICE_{state} is required to appropriately select pure electric or hybrid operation for the current time instant based on instantaneous values of vehicle speed, required output power and operating mode in the previous time instant as specified in the control workflow illustrated in Figure 3. It should be noted that monitoring the value of battery SOC for the Ego HEV would be required as well in order to evaluate battery SOC dependent parameters (e.g. internal resistance, open-circuit voltage) and to determine the torque split between ICE and MG. An additional state variable for the Ego vehicle battery SOC would be in turn required. However, this approach would lead to exponentially increase the associated computational effort, which currently represents a well-known drawback of the DP technique named curse of dimensionality. The capability of executing the developed DP tool for solving the V2V autonomous driving problem on a common desktop computer might consequently be compromised. To overcome this issue, a different approach is implemented here in forecasting the battery SOC profile over time for the Ego HEV based on the simulation of the Lead HEV previously performed. Details regarding this procedure will be provided in the next section.

A generic DP Matlab® toolbox has been used in this work made available from Sundstrom and Guzzella [32]. The initial values of

state variables are set to 20m for the IVD and to 0m/s for the Ego vehicle longitudinal speed, while the value of the state variable associated to the IVD is limited within instantaneous allowed values as discussed in the previous sub-section. Since the retained DP tool allows constraining final values of state variables as well [33], the final IVD has been set here to be below 20m in order to guarantee that the Ego vehicle travels at least the same mileage as the Lead vehicle.

4. Simulation results

This section aims at illustrating simulation results obtained for the P2 HEV in different driving profiles travelling both as Lead vehicle (i.e. following the speed profile of the given drive cycle) and as Ego vehicle (i.e. following the speed profile generated by the introduced V2V autonomous driving optimal control approach). To this end, the workflow illustrated in Figure 5 is implemented to provide a dedicated evaluation framework.

The drive cycle speed profile is retained first as input along with HEV data and related on-board control logics as illustrated in Section 2 in this paper. Step 1 in Figure 5 then involves simulating the operation of the Lead HEV driving through the retained cycle. Overall estimated fuel consumption and the battery SOC trajectory can be evaluated in this way for the Lead P2 HEV. As mentioned earlier, the battery SOC trajectory for the Lead HEV can then be used as forecasted SOC that represents input to the DP control optimization related to the Ego HEV automated V2V autonomous driving. This approach stems from two main assumptions: (1) Lead HEV and Ego HEV exhibit the same value of battery SOC at the beginning of the ride; (2) instantaneous values of battery SOC throughout the drive cycle might be comparable between Lead HEV and Ego HEV due to similarity in terms of vehicle, powertrain architecture, control logic and driving profile. During Step 2 in Figure 5, the longitudinal speed profile to be followed by the Ego vehicle in the entire driving mission is evaluated off-line by the DP approach discussed in Section 3.2 in this paper by solving the related optimal V2V autonomous driving problem illustrated in Section 3.1. The obtained vehicle speed profile can then be used as input to simulate the related P2 HEV travelling as automated Ego vehicle in V2V driving mode. Related Ego vehicle performance can thus

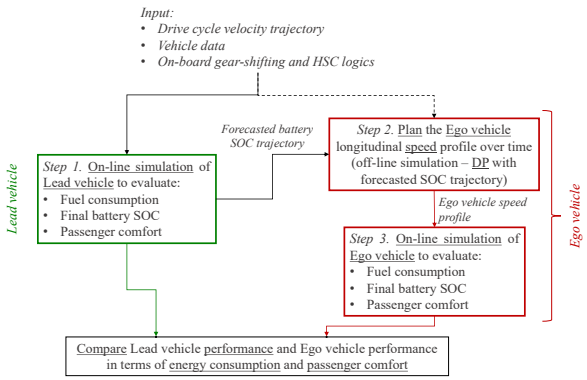

Figure 5. Simulation workflow for evaluating the performance of both Lead vehicle and Ego

be assessed in terms of estimated fuel consumption, battery SOC trajectory, vehicle longitudinal acceleration and other metrics. In this framework, the coefficient α mentioned in equation (5) has been tuned by trial-and-error to achieve a fair trade-off between respective improvements in fuel economy and passenger comfort.

Four drive cycles are considered in this work to demonstrate the effectiveness of the proposed optimal V2V autonomous driving approach for the Ego vehicle in different driving conditions. These include the urban dynamometer driving schedule (UDDS), the worldwide harmonized light-vehicle test procedure (WLTP), the highway federal test procedure (HWFET) and the US06 supplemental procedure (US06). Obtained simulation results for all the retained drive cycles in terms of estimated fuel consumption, net battery energy consumption and RMS of the vehicle acceleration are reported in Table 3. In order to achieve a fair comparison for the fuel economy performance, the amount of fuel needed to recharge the battery up to the initial SOC value (i.e. 60% in this case) needs to be calculated and added to the previously calculated fuel consumption. A method to evaluate this additional fuel consumption has been retained from literature and applied to the specific HEV architecture under analysis [34].

The percentages of performance improvements for the Ego vehicle compared with the Lead vehicle are both reported in Table 3 and illustrated in Figure 6. In general, the proposed optimal control approach for the Ego vehicle in V2V automated driving

Table 3. Simulation results for Lead P2 HEV and Ego P2 HEV in different driving conditions

Drive cycle	Lead vehicle				Ego vehicle			
	Fuel consumption [g]	Battery energy consumption [kWh]	Fuel economy (final SOC correction) [l/100km]	RMS ($\ddot{x}$) [m/s^2]	Fuel consumption [g]	Battery energy consumption [kWh]	Fuel economy (final SOC correction) [l/100km]	RMS ($\ddot{x}$) [m/s^2]
WLTP	1565.7	0.26	9.42	0.53	1523.9	0.28	9.17 (-2.6%)	0.38 (-28.6%)
UDDS	605.1	0.26	7.48	0.63	588.2	0.31	7.29 (-2.6%)	0.48 (-23.8%)
HWFET	1064.8	0.13	8.92	0.30	1053.5	0.13	8.83 (-1.1%)	0.25 (-17.0%)
US06	1002.0	0.30	11.20	0.99	954.8	0.33	10.70 (-4.5%)	0.75 (-23.7%)

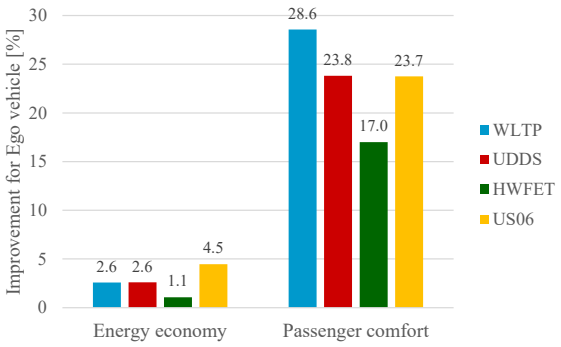

Figure 6. Improvements achieved by the Ego vehicle compared with the Lead vehicle in terms if energy economy and passenger comfort

reveals its effectiveness in improving both fuel economy and passenger comfort for the retained HEV in all driving conditions considered. A peak of 4.5% energy economy improvement for the Ego vehicle can particularly be observed in aggressive driving conditions such as in US06. On the other hand, following the proposed approach, highway driving conditions (such as in HWFET) for the Lead vehicle reflect in limited improvement for the corresponding energy economy of the Ego vehicle that amounts to 1.1%. As far as the passenger comfort is concerned, the highest performance improvement for the Ego vehicle is estimated to be achieved in mixed conditions such as in WLTP. This correlates with a 28.3% reduction in the RMS of the Ego vehicle acceleration compared with the RMS of the Lead vehicle acceleration. UDDS and US06 immediately follow WLTP in the ranking of driving conditions that offer potential of passenger comfort improvement through V2V autonomous driving according to the introduced Ego vehicle speed controller. Finally, HWFET is characterized by reduced opportunity also regarding passenger comfort improvement that is limited to around 17%.

A breakdown of the different factors contributing to vehicle losses reduction for the Ego vehicle compared with the Lead vehicle is shown in Figure 7 in terms of road load, MG loss, battery loss and ICE chemical loss for all the retained driving missions. On the other hand, Figure 8 shows simulation results in terms of time series of IVD, gear number, vehicle speed, consumed fuel and battery SOC for both Lead vehicle and Ego vehicle in WLTP. The reduction in ICE chemical loss for the Ego vehicle compared with the Lead vehicle appears to be the predominant contribution to fuel economy improvement in all driving conditions in Figure 7. This term is evaluated by integrating the difference between fuel power and ICE mechanical power throughout the entire drive cycle. Thanks to automated driving for the Ego vehicle as controlled by the proposed DP approach, up to around 37Wh/km of ICE chemical loss reduction can be achieved in US06 compared with the Lead vehicle following the corresponding drive cycle. This might relate both to the reduction in overall mechanical energy that needs to be provided by the ICE throughout the ride and to the increase in general ICE efficiency. The road load term in Figure 7 is affected by the rolling resistance, the aerodynamic drag, and other miscellaneous terms related to vehicle body and chassis, and it depends on the value of vehicle speed as reported in equation (1). The introduced DP based Ego vehicle controller generally entails smoothing time series and cutting peak values for the Ego vehicle speed compared with the Lead vehicle speed as shown as example in Figure 8 for UDDS. In Figure 7, around 3Wh/km reduction in vehicle loss due to road load can thus be achieved on average as consequence of the smoother driving conditions identified by DP for the Ego vehicle longitudinal speed compared with the corresponding drive cycle followed by the Lead vehicle. Lower and more constant values of vehicle speed over time for the Ego vehicle reflect as well in the reduction of MG loss and battery loss. Instantaneous MG loss can be calculated by interpolation in the corresponding lookup table as function of MG speed and torque, and corresponding reduction for the Ego vehicle compared with the Lead vehicle range from 1.4Wh/km in HWFET to 7.0Wh/km in US06. On the other hand,

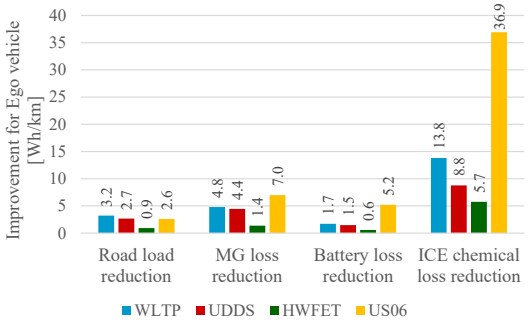

Figure 7. Breakdown of vehicle losses reduction achieved by the Ego vehicle compared with the Lead vehicle

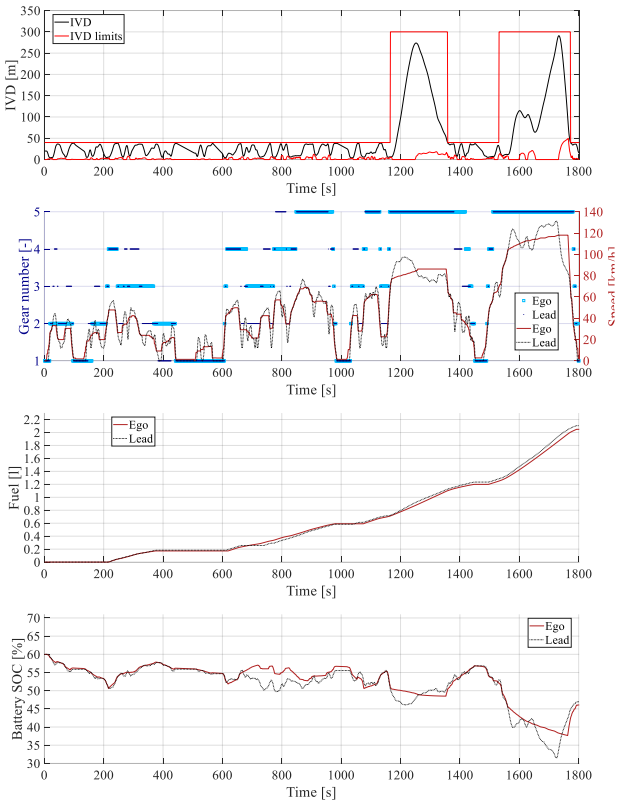

Figure 8. Simulated time series of IVD, gear number, vehicle speed, consumed fuel and battery SOC for both Lead vehicle and Ego vehicle in WLTP

instantaneous battery loss can be calculated by multiplying the internal resistance by the squared value of the battery current. The battery loss term is observed in Figure 7 impacting around 0.6Wh/km to around 5.2Wh/km in the Ego vehicle loss reduction compared with the Lead vehicle. An overview regarding how different factors contribute to improving the on-board energy management of the Ego HEV is provided in this way.

5. Conclusions

This paper has presented a methodology that allows generating longitudinal velocity profiles for an Ego parallel P2 HEV travelling behind a Lead vehicle in V2V automated driving. The presented off-line controller for the Ego HEV longitudinal acceleration over time relies on the principle of global optimality achieved by DP. The DP control objectives for the Ego HEV include both the overall tractive energy and the RMS of the vehicle acceleration, which aim at respectively enhancing fuel economy and passenger comfort. The on-board hybrid supervisory control logic for the HEV is integrated in the DP optimization framework to allow improving energy management.

The effectiveness of the proposed longitudinal velocity planner for the Ego vehicle has been demonstrated through simulations in different driving conditions. The HEV performance when travelling as Ego vehicle has been benchmarked with the corresponding performance when following the drive cycle as Lead vehicle. Mixed and aggressive driving conditions have been identified as the most promising ones both in terms of fuel economy enhancement and passenger comfort improvement by V2V automated driving according to the proposed approach. On the other hand, when the Lead vehicle encounters highway driving conditions, remarkable improvements might be achieved only in passenger comfort, while limited saving might be attained in terms of fuel consumption according to the described methodology.

Different possible directions might be suggested here for related future work. First, adapting the hybrid supervisory controller when the HEV travels as Ego vehicle in V2V automated driving could be performed to further enhancing fuel economy improvement. A nested approach could particularly be implemented for the simultaneous optimization of Ego HEV velocity profile and energy management. Moreover, real-time velocity planners could be developed to be on-board implemented in the Ego HEV based on the off-line results provided here by DP. Finally, estimating the optimal fuel economy achievable in V2V autonomous driving according to the proposed methodology could be integrated as criterion for advanced powertrain design and sizing procedure for automated HEVs.

References

[1] Anselma, P. and Belingardi, G., "Next Generation HEV Powertrain Design Tools: Roadmap and Challenges," *SAE Technical Paper* 2019-01-2602, 2019.

[2] T. Plum, M. Wegener, M. Eisenbarth, Z. Ye, K. Etzold, S. Pischinger, J. Andert, “A simulation-based case study for powertrain efficiency improvement by automated driving functions”, *Proc. Inst. Mech. Eng., Part D: J. Automobile Eng*, vol. 223, no. 5, pp. 1320-1330, 2018.

[3] Chen, Y., Chamadiya, B., and Bueker, U., "V2V Communication - Analysis and Validation of Propagation Models in Real World Scenarios," *SAE Technical Paper* 2015-01-0289, 2015.

[4] Moser, D., Waschl, H., Schmied, R., Efendic, H. et al., "Short Term Prediction of a Vehicle's Velocity Trajectory Using ITS," *SAE Int. J. Passeng. Cars – Electron. Electr. Syst.*, 8(2):2015.

[5] IEEE, “Toyota and Lexus to launch DSRC technology to connect vehicles and infrastructure in the U.S. in 2021,” 2018. [Online]. http://sites.ieee.org/connected-vehicles/2018/04/16/toyota-and-lexus-to-launch-dsrc-technology-to-connect-vehicles-and-infrastructure-in-the-u-s-in-2021/, accessed 21 Apr. 2020.

[6] P.G. Anselma, G. Belingardi, “Comparing Battery Electric Vehicle Powertrains through Rapid Component Sizing”, in *International Journal of Electric and Hybrid Vehicles*, vol. 11, no. 1, pp. 36-58, 2019.

[7] Anselma, P., Huo, Y., Amin, E., Roeleveld, J. et al., "Mode-shifting Minimization in a Power Management Strategy for Rapid Component Sizing of Multimode Power Split Hybrid Vehicles," *SAE Technical Paper* 2018-01-1018, 2018.

[8] F. Zhang, J. Xi and R. Langari, "Real-Time Energy Management Strategy Based on Velocity Forecasts Using V2V and V2I Communications," in *IEEE Transactions on Intelligent Transportation Systems*, vol. 18, no. 2, pp. 416-430, Feb. 2017.

[9] Plianos, A., Jokela, T., and Hancock, M., "Predictive Energy Optimization for Connected and Automated HEVs," *SAE Technical Paper* 2018-01-1179, 2018.

[10] Baker, D., Asher, Z.D., and Bradley, T., “V2V Communication Based Real-World Velocity Predictions for Improved HEV Fuel Economy,” *SAE Technical Paper* 2018-01-1000, 2018.

[11] P.G. Anselma, G. Belingardi, A. Falai, C. Maino, F. Miretti, D. Misul, E. Spessa, “Comparing Parallel Hybrid Electric Vehicle Powertrains for Real-world Driving”, *2019 AEIT International Conference of Electrical and Electronic Technologies for Automotive*, Torino, Italy, 2019, pp. 1-6.

[12] Dabadie, J., Sciarretta, A., Font, G., and Le Berr, F., "Automatic Generation of Online Optimal Energy Management Strategies for Hybrid Powertrain Simulation," *SAE Technical Paper* 2017-24-0173, 2017.

[13] G. Alix, J. Dabadie, G. Font, “An ICE Map Generation Tool Applied to the Evaluation of the Impact of Downsizing on Hybrid Vehicle Consumption”, *SAE Technical Paper* 2015-24-2385, 2015.

[14] F. Le Berr, A. Abdelli, D.-M. Postariu, R. Benlamine, “Design and Optimization of Future Hybrid and Electric Propulsion Systems: An Advanced Tool Integrated in a Complete Workflow to Study Electric Devices”, *Oil & Gas Science and Technology*, vol. 67, no. 4, pp. 547-562, 2012.

[15] M. Petit, N. Marc, F. Badin, R. Mingant and V. Sauvant-Moynot, “A Tool for Vehicle Electrical Storage System Sizing and Modelling for System Simulation”, *2014 IEEE Vehicle Power and Propulsion Conference (VPPC)*, Coimbra, 2014, pp. 1-5.

[16] L. Guzzella and A. Amstutz, "CAE tools for quasi-static modeling and optimization of hybrid powertrains," in *IEEE Transactions on Vehicular Technology*, vol. 48, no. 6, pp. 1762-1769, 1999.

[17] P. G. Anselma, A. Biswas, J. Roeleveld, G. Belingardi and A. Emadi, "Multi-Fidelity Near-Optimal on-Line Control of a Parallel Hybrid Electric Vehicle Powertrain," *2019 IEEE*

Transportation Electrification Conference and Expo (ITEC), Detroit, MI, USA, 2019, pp. 1-6.

[18] A. Biswas and A. Emadi, "Energy Management Systems for Electrified Powertrains: State-of-the-Art Review and Future Trends," in *IEEE Transactions on Vehicular Technology*, vol. 68, no. 7, pp. 6453-6467, July 2019.

[19] D. Zhu, H. Chen, S. Zhu and G. Yang, "Optimization of control parameters for a parallel hybrid electric vehicle based on AMESim," *2014 IEEE Conference and Expo Transportation Electrification Asia-Pacific (ITEC Asia-Pacific)*, Beijing, 2014, pp. 1-4.

[20] X. Li and S. A. Evangelou, "Torque-Leveling Threshold-Changing Rule-Based Control for Parallel Hybrid Electric Vehicles," in *IEEE Transactions on Vehicular Technology*, vol. 68, no. 7, pp. 6509-6523, July 2019.

[21] E. Paschalidis, F. Hajiseyedjavadi, C. Wei, A. Solernou, A.H. Jamson, N. Merat et al., "Deriving metrics of driving comfort for autonomous vehicles: A dynamic latent variable model of speed choice", *Analytic Methods in Accident Research*, vol. 28, no. 100133, 2020.

[22] S. Feraco, S. Luciani, A. Bonfitto, N. Amati and A. Tonoli, "A local trajectory planning and control method for autonomous vehicles based on the RRT algorithm," *2020 AEIT International Conference of Electrical and Electronic Technologies for Automotive (AEIT AUTOMOTIVE)*, 2020, pp. 1-6.

[23] D. He, W. He, X. Song, "Efficient predictive cruise control of autonomous vehicles with improving ride comfort and safety", *Measurement and control*, vol. 53, no. 1-2, pp. 18-28, 2020.

[24] S. Luciani, A. Bonfitto, N. Amati, A. Tonoli, "Model predictive control for comfort optimization in assisted and driverless vehicles", in *Advances in Mechanical Engineering,* vol. 12, no. 11, pp.1-14, 2020.

[25] P.G. Anselma, G. Belingardi, "Enhancing Energy Saving Opportunities through Rightsizing of a Battery Electric Vehicle Powertrain for Optimal Cooperative Driving", *SAE Intl. J. CAV*, vol. 3, no. 2, 2020.

[26] U.S. Department of Energy, "Nhtsa Issues Advance Notice of Proposed Rulemaking and Research Report on Ground-Breaking Crash Avoidance Technology: "Vehicle-Tovehicle Communications: Readiness of V2V Technology For Application", *Vehicle-to-vehicle Communication Technology*, [online] available: https://www.nhtsa.gov/sites/nhtsa.dot.gov/files/documents/v2v_fact_sheet_101414_v2a.pdf (accessed 21 Apr. 2021).

[27] C. Chen, N. Lü, L. Liu et al., "Critical safe distance design to improve driving safety based on vehicle-to-vehicle communications", *J. Cent. South Univ.*, vol. 20, no.11, pp. 3334-3344, 2013.

[28] R. Bellman and R. Kalaba, "Dynamic programming and adaptive processes: Mathematical foundation," in *IRE Transactions on Automatic Control*, vol. AC-5, no. 1, pp. 5-10, Jan. 1960.

[29] J. Ogrzewalla, M. Stapelbroek , J. Pfluger, T. Plum, "Dynamic Speed Trajectory Optimization for Achieving Real World Optimum Energy Consumption", *FISITA 2016 World Automotive Congress*, Busan, Korea, 2016.

[30] L. Bruck, A. Lempert, S. Amirfarhangi Bonab, J. Lempert et al., "A Dynamic Programming Algorithm for HEV Powertrains Using Battery Power as State Variable," *SAE Technical Paper* 2020-01-0271, 2020.

[31] C. Mansour, R. Khairallah, B. Kabalan, "Optimized Rule-based Energy Management Strategy for the Toyota Prius Plug-in Hybrid using Dynamic Programming", *FISITA 2014 World Automotive Congress*, Maastricht, Netherlands, 2014.

[32] O. Sundstrom and L. Guzzella, "A generic dynamic programming Matlab function," *2009 IEEE Control Applications, (CCA) & Intelligent Control, (ISIC)*, St. Petersburg, Russia, 2009, pp. 1625-1630.

[33] P. Elbert, S. Ebbesen and L. Guzzella, "Implementation of Dynamic Programming for n-Dimensional Optimal Control Problems With Final State Constraints," in *IEEE Transactions on Control Systems Technology*, vol. 21, no. 3, pp. 924-931, May 2013.

[34] N. Ligterink et al., "Correction algorithms for WLTP chassis dynamometer and coast-down testing", *TNO-rapport 2015 R10955*, 2015.